Radiative properties of upper tropospheric clouds observed by Aura MLS and CloudSat

Hui Su[1], Jonathan H. Jiang[1], Graeme L. Stephens[2], Deborah G. Vane[1] and Nathaniel Livesey[1]

[1]Jet Propulsion Laboratory, California Institute of Technology, Pasadena, CA, 91109, USA

[2]Department of Atmospheric Science, Colorado State University, Fort Collins, CO, 80523, USA

Corresponding author address: Dr. Hui Su, Jet Propulsion Laboratory, California Institute of Technology, Pasadena, CA, 91109, USA.

Email: Hui.Su@jpl.nasa.gov

Copyright 2009. All rights reserved.

Abstract. The radiative properties of upper tropospheric clouds observed by CloudSat and Aura MLS are examined and contrasted. We find that the occurrence frequency of thin cirrus clouds (TCC) detected by MLS but missed by CloudSat is about 4-10% on average in the tropical tropopause layer (TTL) and 40~60% near the tropopause in the deep convection regions. The TCC typically have visible optical thickness less than 0.2. Their tropical-mean top-of-atmosphere cloud forcing is 3.5 W/m^2 net warming. Locally, they can produce a warming of ~20 W/m^2. The TCC creates 1.2 W/m^2 cooling at the surface. In the TTL, the radiative heating rates induced by the TCC are ~0.35 K/day in the tropical-mean, and about 0.8 K/day in the South Asia summer monsoon region, which is 3-4 times the clear-sky radiative heating rate. Hence, they are potentially important in affecting the TTL mass transport rates.

1. Introduction

Clouds cool the Earth by reflecting solar radiation and warm the Earth by trapping thermal emissions. For high-altitude clouds, their longwave (LW) and shortwave (SW) effects can be comparable in magnitude, making their net effect more uncertain than lower-altitude clouds. Thin cirrus clouds tend to have a net warming as their greenhouse effect overcomes their albedo effect, while thick cirrus anvils may tend to have a net cooling [e.g. *Stephens et al.*, 1990; *Ramanathan and Collins*, 1991]. The radiative heating/cooling rate induced by cirrus clouds in the tropical tropopause layer (TTL) has also been considered an important factor in affecting mass transport from the troposphere to the stratosphere [e.g. *Hartmann et al.*, 2001; *Corti et al.,* 2006]. Accurate quantification of cirrus radiative effects relies on accurate measurements of cirrus cloud profiles. This is now possible with the advent of the NASA A-train satellite instruments, in particular, CloudSat, CALIPSO, and Aura Microwave Limb Sounder (MLS).

CloudSat provides a global survey of tropospheric cloud profiles with a nadir-viewing 94 GHz Cloud Profiling Radar. The global cloud liquid and ice water content (L/IWC) profiles are retrieved based on the empirical log-linear relationship between the radar reflectivity (Z_e) and L/IWC when $Z_e \geq -31$ dBz [*Austin et al*., 2008]. Hence, CloudSat cannot detect thin cirrus of small IWC and non-precipitating liquid clouds of small LWC. Aura MLS measures upper tropospheric (UT) ice clouds at ~11km (215hPa) and higher using a 240 GHz radiometer [*Wu et al*., 2008]. It can detect some thin cirrus that is below CloudSat detection limit. The CALIPSO lidar, operating at 532 nm and 1064 nm, can detect even thinner clouds than MLS. *Haladay and Stephens* [2008, hereafter HS08] analyzed joint observations from CloudSat and CALIPSO for June, July, and August (JJA) 2006. They found the thin ice clouds detected by CALIPSO but missed by CloudSat have a cloud cover of ~25% in the tropics (20ºS-20ºN). Their optical depth

ranged between 0.02-0.3. These thin clouds produced less than 2 W/m^2 shortwave cooling and ~20 W/m^2 longwave warming at the top-of-atmosphere (TOA) instantaneously, with tropical-mean atmospheric heating of ~4 W/m^2. In this study, we compare the UT cirrus observations from MLS and CloudSat, and perform radiative transfer calculations using these data as inputs. Our aim is to quantify how much more thin cirrus clouds are detected by MLS than by CloudSat and what are the radiative effects at TOA and the surface of these additional clouds, as well as their radiative heating rates in the atmosphere. This study enables users of both datasets to have a quantitative view of the consistency and discrepancy of these measurements, and the advantages and limitations of each instrument.

2. Datasets

We analyze data during JJA 2008, the same season as in HS08, chosen because the Aura and CloudSat/CALIPSO orbits have been aligned within ~10 km in terms of equatorial cross position over that period. Prior to May 2008, the Aura MLS track was about 200 km away from the CloudSat/CALIPSO tracks, making a direct comparison of the cloud scenes difficult. The CloudSat IWC/LWC is taken from the Level 2B R04 dataset [*Austin et al.*, 2008], with a horizontal resolution of 1.7 km along-track and 1.3 km cross-track. The vertical resolution is ~500 m. The MLS IWC is from the Level 2 v2.2 product, with a horizontal resolution of ~200 km along-track and ~7 km cross-track. The vertical resolution is ~3 km [*Wu et al.*, 2008]. When comparing the 3-month mean cirrus distributions, we average both CloudSat and MLS data onto the same 8º (longitude) × 4º (latitude) × 3 km (height) grids. For radiation calculations, we average the CloudSat IWC onto 2º×0.2º areas centered on the MLS measurement locations (approximately matching the MLS footprints) and run the radiative transfer model along the MLS tracks. Then radiative fluxes and heating rates are gridded onto 8º×4º boxes for horizontal maps.

The Fu-Liou radiative transfer model is used [*Fu and Liou*, 1993]. For atmospheric temperature, we use the data from Atmospheric Infrared Sounder (AIRS) on Aqua satellite (Level 3, 1º×1º horizontal resolution) averaged onto the approximate MLS footprints, same as for the CloudSat data. For water vapor, we use AIRS H_2O up to 200 hPa and MLS H_2O above because the AIRS retrieved H_2O degrades in the higher altitudes [*Fetzer et al.*, 2008]. The ozone profile is based on the standard tropical atmosphere. The sea surface temperature (SST) is from the Advanced Microwave Scanning Radiometer (AMSR-E) (0.25º×0.25º resolution) on Aqua. The land surface albedo data are taken from the Moderate Resolution Imaging Spectroradiometer (MODIS) Filled Land Surface Albedo Product at 0.3-0.7 μm wavelength. Both SST and albedo are interpolated onto the MLS measurement locations. To evaluate the calculated radiative fluxes, we compare our model results with the Clouds and the Earth's Radiant Energy System (CERES) Energy Balanced and Filled (EBAF) 5-year climatology (March 2000 to October 2005) of TOA radiative fluxes [*Wielicki et al*., 1996] and zonal-mean surface radiative flux estimates based on the International Satellite Cloud Climatology Project (ISCCP) [*Zhang et al.*, 2004] and Global Energy and Water Cycle Experiment-Surface Radiation Budget (GEWEX-SRB) project [*Raschke et al.*, 2006].

3. CloudSat and MLS Observed Cirrus Distributions

We first derive cloud occurrence frequency in the UT during JJA 2008 by dividing the number of cloudy measurements by the number of total measurements in each 8º (longitude) × 4º (latitude) × 3 km (height) volume. Figure 1 (left panels) displays the maps of the 3-month mean cloud occurrence frequency at 11 km, 13 km, and 16 km for CloudSat and the difference between MLS and CloudSat (MLS minus CloudSat) in the tropics (30ºS-30ºN). At 16 km, MLS produces higher UT cloud occurrence frequency than CloudSat ubiquitously. The thin cirrus clouds captured by MLS but missed by CloudSat (shorthanded as TCC) mostly occur in the deep convective regions,

with a pronounced high occurrence of 40-60% over the South Asia monsoon region. At 13 km, MLS also yields higher cloud occurrence than CloudSat in the convection centers, but MLS underestimates cloud occurrence in certain areas such as the western Indian Ocean, North Pacific and Atlantic, and South Pacific. The MLS underestimate of cloud occurrence is also clear at 11 km. This could be due to the coarse resolution of MLS observations and/or saturation of cloud signal when IWC > 50-120 mg/m^3 (depending on heights) [*Wu et al.*, 2008]. The average TCC occurrence frequency within 30°S-30°N is about 10%, 4% and 6% at 16 km, 13 km and 11 km, respectively.

We also compared the IWC values from MLS and CloudSat for this period. CloudSat and MLS retrieved IWC have similar morphology, but the CloudSat IWC values are generally larger than MLS by a factor of 2 or greater, possibly due to the different cloud particle size assumptions for the IWC retrievals. Our results are similar to *Wu et al.* [2008, their Figure 6].

We calculated the visible (0.2-0.7 μm) optical thickness (τ) of the UT (pressure ≤ 215 hPa) cirrus clouds using the Fu-Liou radiative transfer model with CloudSat and MLS IWC as inputs. The cloud particle size is calculated as a function of the observed IWC and AIRS temperature based on the size distribution parameterization by *McFarquhar and Heymsfield* [1997]. We run the model for three cases. The first case, the "Control" run, uses MLS IWC at 215 hPa and higher altitudes combined with CloudSat L/IWC below 215hPa. The second case, the "CloudSat" run, uses only CloudSat L/IWC throughout the atmospheric column. The third case, the "Max" run, uses the larger value of CloudSat and MLS IWC at the same height. This run attempts to identify the impact of the IWC retrieval bias between CloudSat and MLS. It gives an upper bound of the ice cloud amount when the maximum possible IWC retrievals are used. The probability density functions (PDF) of the calculated τ in the UT for the three cases are shown in the right panel of

Figure 1. The "Control" run and the "CloudSat" run have substantially different PDFs of τ while the "Max" run is almost identical to the "Control" run except when $\tau > 1$. The optical thickness of TCC ranges from 0.01 to 0.2, with a peak distribution around $\tau = 0.023$. The PDF of τ in the "CloudSat" run peaks around τ=0.04, below which CloudSat loses sensitivity. The cumulative distribution for $\tau \leq 0.2$ is 0.71 for the "Control" run, 0.34 for the "CloudSat" run and 0.70 for the "Max" run. When $\tau > 0.2$, the "CloudSat" run has a higher PDF than the "Control" run. Compared to HS08, our calculated τ is somewhat smaller than their estimates based on CALIPSO lidar backscatter, partly because we limit the calculations to cloud altitudes above 215 hPa. It may also be due to different cloud particle size assumptions.

4. Cloud Radiative Forcing at TOA and at the Surface

We define cloud radiative forcing (CRF) as the difference between all-sky and clear-sky radiative fluxes at TOA and the surface, with positive sign representing warming the atmosphere or the surface. Three model runs with different UT IWC inputs as described in the previous section are conducted. The "Control" run serves as a baseline experiment and is compared to CERES and ISCCP data in detail for evaluation of the radiative transfer calculations. The differences between the "Control" run and the other two runs thus illustrate the CRFs caused by the different UT IWCs.

Figure 2 shows the TOA LW, SW and net CRF for the CERES climatology, the "Control" run and the difference between the "Control" run and the "CloudSat" run. The results for the "Max" run are very similar to the "Control" run and thus not shown. The tropical-mean (30ºS-30ºN) CRFs at TOA and the surface for observations and the three model runs are listed in Table 1. For CRF at the surface, direct observations are difficult and the available "observational" data are either calculated from radiative transfer models using observed atmosphere and cloud profiles as inputs or based on empirical relations between TOA and surface radiative fluxes. As CRF at the surface

is not available from CERES EBAF data, we use the tropical-mean TOA and surface CRF estimates from ISCCP [*Zhang et al.*, 2004] in Table 1 for observations. The ISCCP surface CRF estimates came from radiative transfer model calculations with the best available atmospheric state variables and ISCCP cloud information as inputs for the period of 1984 to 2004. A rough specification of uncertainties for each term is given according to *Zhang et al.* [2004] and *Raschke et al.* [2006].

In Figure 2, the TOA CRFs in the "Control" run compare fairly well with the CERES climatology, which is regridded from the original 1º×1º to the same 8º×4º grids as the model results. Large cloud forcings are found over the convective centers, including Western Pacific, South Asian monsoon region, central Africa and America, and inter-tropical convergence zone (ITCZ). The modeled LW CRF is somewhat weaker than CERES. This may reflect contributions from even thinner cirrus not captured by MLS. Over land, a constant surface skin temperature of 300 K was used in the model calculations, which may also introduce errors in LW CRF. The tropical mean LW CRF at TOA in the "Control" run is 21.7 W/m^2, about 7.5 W/m^2 smaller than that of CERES EBAF 5-year climatology and about 5 W/m^2 smaller than the ISCCP average for 1984-2004 (Table 1). The TOA SW CRF in the "Control" run is similar to CERES in morphology and amplitude. The major deficiency is in the west coast of California, likely due to the underestimate of stratiform clouds by CloudSat there. The tropical-mean SW CRF at TOA is –46.9 W/m^2 in the "Control" run, comparable to CERES EBAF, –44.0 W/m^2, and ISCCP, –48.0 W/m^2 (Table 1). The net CRF at TOA for the "Control" run is in the ballpark of CERES and ISCCP climatology.

At the surface, the tropical-mean LW warming in the "Control" run is smaller than the ISCCP estimate by ~10 W/m^2. This may be due to the land surface temperature specification and

underestimate of cloud amount. *Zhang et al.* [2006] showed that 2-3 K uncertainty in surface skin and air temperature can translate into 10-15 W/m^2 uncertainty in the surface LW flux. The modeled SW cooling at the surface is similar to the ISCCP estimate. Thus, the net CRF at the surface in the "Control" run shows a larger net cooling than ISCCP.

Given the reasonable comparison between the "Control" run and the CERES and ISCCP data, we focus our attention to the differences of CRFs between the "Control" run and the "CloudSat" run. These differences are primarily contributed by TCC. Shown in Figure 2g-i, the additional LW CRF at TOA caused by TCC is up to 20 W/m^2 in the deep convective regions. TCC also increase TOA SW cooling with amplitude less than 5 W/m^2. Hence, adding the missed TCC to the CloudSat measurements would increase TOA net warming by ~15 W/m^2 in the deep convective regions, with a tropical-mean net warming of 3.5 W/m^2 (4.7 W/m^2 LW warming and −1.2 W/m^2 SW cooling). However, TCC have a relatively weak impact on the surface radiative energy budget. The tropical-mean LW and SW CRFs at the surface by TCC are 0.1 and −1.3 W/m^2, respectively, resulting in −1.2 W/m^2 net cooling (Table 1).

In the "Max" run, the CRFs at TOA and at the surface are quite similar to the "Control" run, with a slight increase about 1 W/m^2. This is not surprising as indicated by the comparison of τ in Figure 1. It suggests that the missed detection of thin cirrus plays a significant role in determining the cloud radiative effects, and the IWC retrieval bias has a relatively small impact.

5. Cloud-induced Radiative Heating Rate

Figure 3 shows the cloud-induced radiative heating rate (CHR, all-sky minus clear-sky heating rates) from the three runs averaged over the tropics (30°S-30°N) and the South Asia monsoon region (10°S-30°N, 60°E-150°E). The tropical-mean CHR is positive over most of the troposphere, except in the boundary layer between 900 and 800 hPa. There is also small cooling in

the lower stratosphere due to the LW emission from the cold cloud tops. In the TTL, there is a marked enhancement of cloud radiative heating when combined MLS and CloudSat IWC are used compared to using CloudSat IWC alone. This heating is largely due to the absorption of solar radiation by cirrus. The tropical-mean CHR at 200 hPa is about 0.15, 0.5 and 0.65 K/day in the "CloudSat", "Control" and "Max" runs, respectively. Over the South Asia monsoon region, the averaged CHR is much larger in the "Control" and "Max" runs than in the "CloudSat" run, consistent with the substantially higher TCC occurrence frequency there (Figure 1). The local radiative heating rate produced by TCC is about 0.8 K/day in the TTL, which is 3-4 times the clear-sky radiative heating rate. As *Corti et al.* [2006] suggested, the larger radiative heating inside the cirrus may provide a faster mass transport pathway for the tracer transport from the troposphere to the stratosphere.

6. Conclusions

This study examines the radiative properties of UT clouds observed by CloudSat and MLS, and compares the TOA and surface cloud forcings and cloud-induced radiative heating rates when different IWC measurements are used. We focus on the effects of the thin cirrus clouds detected by MLS but missed by CloudSat, the TCC. The cloud occurrence reported by CloudSat is about 10% less than MLS near the tropopause in the tropical average and is about 60% lower in the regions of deep convection, such as the South Asia monsoon region. These thin cirrus clouds mostly have optical depth ranging from 0.01 to 0.2. Our radiative transfer calculations show that TCC have a dominantly LW warming effect at TOA. Locally, their LW warming effect at TOA can be as large as 20 W/m^2. On tropical average, they contribute to 3.5 W/m^2 net warming at TOA and -1.2 W/m^2 net cooling at the surface. Our results are consistent with HS08 which estimated the cloud forcings of thin cirrus missed by CloudSat but detected by CALIPSO. A caveat in our

radiation calculations is that we did not consider the variabilities of land surface skin temperature, aerosol composition/concentration, and ozone changes. These factors may introduce errors in the radiative fluxes by 10-15 W/m^2 [e.g. *Zhang et al.*, 2006].

Furthermore, we show that TCC produce a substantial radiative heating in the TTL. Over the South Asia monsoon region, where TCC occur most frequently, the local radiative heating rate is about 0.8 K/day, 3-4 times larger than the clear-sky radiative heating rate. Hence, the thin cirrus may be potentially important in altering the vertical transport rates for TTL tracers entering the stratosphere.

This study demonstrates the importance and benefits of merging multiple satellite cloud measurements for accurate assessment of cloud radiative effects. Combining CloudSat and MLS IWC measurements clearly yields better estimates of cloud forcing and cloud radiative heating rates than using CloudSat data alone. However, we recognize that there remains some thin cirrus missed by CloudSat and MLS combined together. This may be compensated by synthesizing CALIPSO data with CloudSat and MLS. Future work using the three instruments together would hopefully yield a more complete picture of clouds and their radiative effects.

Acknowledgements

We thank the funding support from the JPL R&TD and NASA ROSES ACMAP-AST program. We thank Tristan L'Ecuyer for help with CloudSat data and Yu Gu for help with the Fu-Liou radiative transfer modeling. This work is conducted at the Jet Propulsion Laboratory, California Institute of Technology, under contract with NASA.

References

Austin, R A. et al. (2008), Retrievals of ice cloud microphysical parameters using the CloudSat millimeter-wave radar and temperature, *J. Geophys. Res,* in press.

Corti, T., B. P. Luo, Q. Fu, H. Vomel, and T. Peter (2006), The impact of cirrus clouds on tropical troposphere to stratosphere transport, *Atmos. Chem. Phys.*, 6, 2539–2547.

Fetzer, E. J., et al. (2008), Comparison of Upper Tropospheric Water Vapor Observations from the Microwave Limb Sounder and Atmospheric Infrared Sounder, *J. Geophys. Res.*, 113, D22110, doi:10.1029/2008JD010000.

Fu, Q., and K. N. Liou (1993), Parameterization of the radiative properties of cirrus clouds, *J. Atmos. Sci.*, 50, 2008–2025.

Haladay, T., and G. L. Stephens (2008), Characteristics of tropical thin cirrus clouds deduced from joint CloudSat and CALIPSO observations, *J. Geophys. Res*., submitted.

Hartmann, D. L. et al. (2001), The Heat Balance of the Tropical Tropopause, Cirrus, and Stratospheric Dehydration, *Geophys. Res. Lett*., 28(10), 1969–1972.

McFarquhar, G. M., and A. J. Heymsfield (1997), Parameterization of tropical cirrus ice crystal size distributions and implications radiative transfer: Results from CEPEX, *J. Atmos. Sci.*, 54, 2187–2200.

Ramanathan, V., and W. Collins (1991), Thermodynamics regulation of ocean warming by cirrus clouds deduced from observations of the 1987 El Nino, *Nature*, 351, 27–32.

Raschke, E., et al. (2006): An assessment of radiation budget data provided by the ISCCP and GEWEX-SRB, *Geophys. Res. Lett*, 33, L07812, doi:10.1029/2005GL025503.

Stephens, et al., (1990) The Relevance of the Microphysical and Radiative Properties of Cirrus Clouds to Climate and Climatic Feedback. *J. Atmos. Sci.*, 47, 1742–1754.

Wielicki, B. A., et al. (1996), Clouds and the Earth's Radiant Energy System (CERES), An Earth Observing System Experiment, *Bull. Amer. Meteor. Soc*., 77, 853-868, 1996.

Wu, D. L , et al. (2008), Comparisons of Global Cloud Ice from MLS, CloudSat, and Correlative Data Sets, *J. Geophys. Res.*, in press.

Zhang Y., et al. (2004), Calculation of radiative fluxes from the surface to top of atmosphere based on ISCCP and other global data sets: Refinements of the radiative transfer model and the input data, *J. Geophys. Res.*, 109, D19105, doi:10.1029/2003JD004457.

Zhang, Y. et al. (2006), Comparison of different global information sources used in surface radiative flux calculation: Radiative properties of the near-surface atmosphere, *J. Geophys. Res.*, 111, D13106, doi:10.1029/2005JD006873.

Table Captions

Table 1. Observed (based on ISCCP FD-MPF) and modeled tropical-mean (30ºS-30ºN) cloud radiative forcing (in W/m^2) at the top-of-atmosphere (TOA) and at the surface (SFC). The ISCCP data are June-July-August (JJA) averages from 1984 to 2004, with rough error estimates from *Zhang et al.* [2004] and *Raschke et al.* [2006]. The modeled results are for JJA 2008.

	Observations (ISCCP)	Control Run (MLS+CloudSat)	CloudSat Only	Max of MLS/CloudSat
TOA-LW	26.6±5.0	21.7	17.0	22.8
TOA-SW	-48.0±5.0	-46.9	-45.7	-47.7
TOA-net	-21.4±10.0	-25.2	-28.7	-24.9
SFC-LW	18.9±10.0	8.3	8.2	8.4
SFC-SW	-50.0±10.0	-51.6	-50.3	-52.6
SFC-net	-31.1±20.0	-43.3	-42.1	-44.2

Figure Captions

Figure 1. (left two panels) Maps of cloud occurrence frequency at three upper tropospheric levels during June-July-August 2008 from CloudSat, and the difference between MLS and CloudSat data; (right panel) the probability density functions of the optical thickness of clouds based at 215 hPa and higher for the "Control", "CloudSat" and "Max" runs.

Figure 2. The observed and modeled longwave, shortwave and net cloud radiative forcings at the top-of-atmosphere. (a)-(c) CERES; (d)-(f) the "Control" run and (g)-(i) the difference between the "Control" run and the "CloudSat" run.

Figure 3. Cloud radiative heating rates in the atmosphere averaged over the tropics (thicker lines) and the South Asia region (thinner lines) for the three runs.

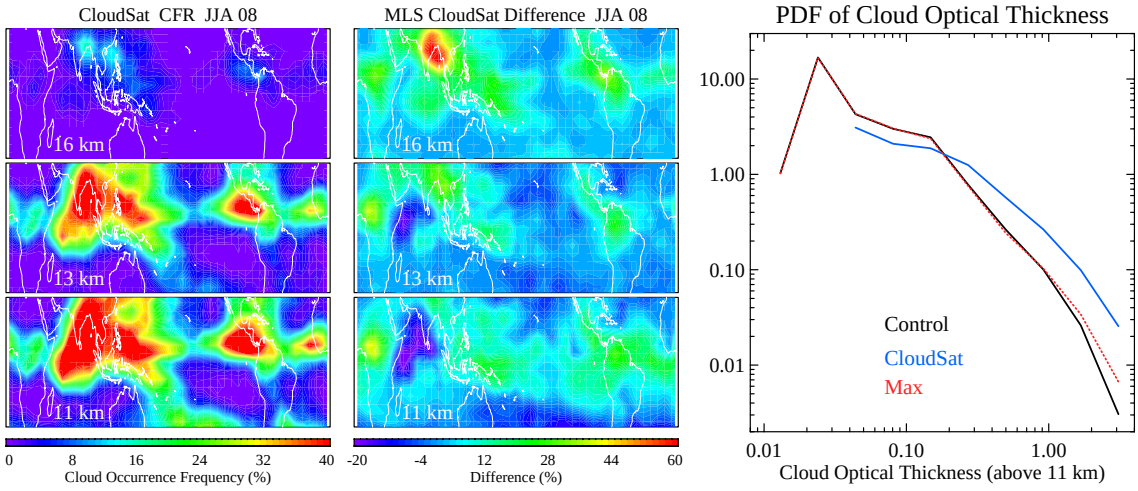
CloudSat CFR JJA 08
MLS CloudSat Difference JJA 08
PDF of Cloud Optical Thickness
16 km
13 km
11 km
0
8
16
24
32
40
Cloud Occurrence Frequency (%)
-20
-4
12
28
44
60
Difference (%)
10.00
1.00
0.10
0.01
Control
CloudSat
Max
0.01
0.10
1.00
Cloud Optical Thickness (above 11 km)

Figure 1

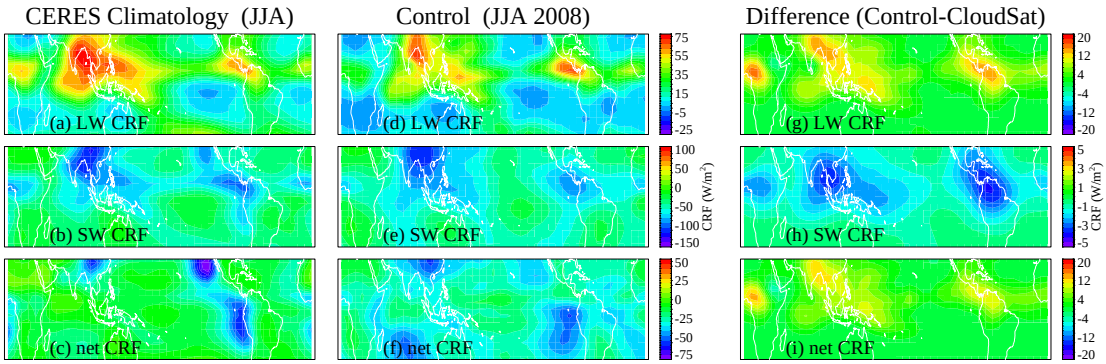
CERES Climatology (JJA)
Control (JJA 2008)
Difference (Control-CloudSat)
(a) LW CRF
(b) SW CRF
(c) net CRF
(d) LW CRF
(e) SW CRF
(f) net CRF
(g) LW CRF
(h) SW CRF
(i) net CRF
CRF (W/m²)

Figure 2

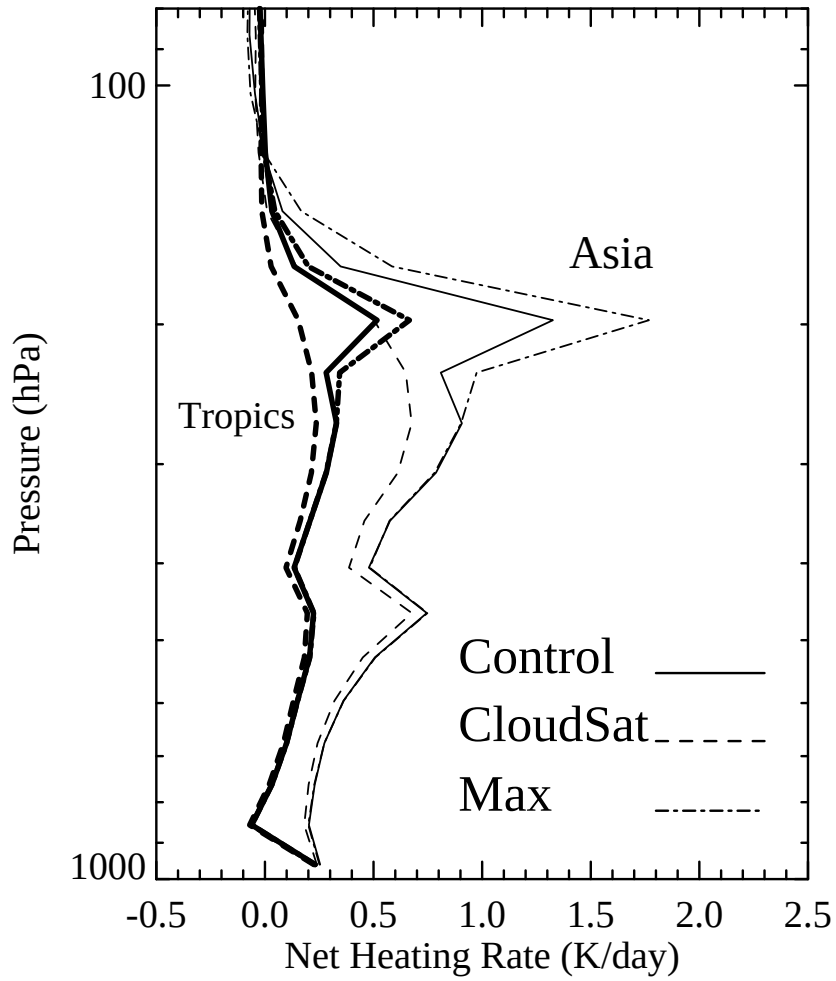
100
1000
Pressure (hPa)
Asia
Tropics
Control
CloudSat
Max
-0.5
0.0
0.5
1.0
1.5
2.0
2.5
Net Heating Rate (K/day)

Figure 3